Macromolecules

ARTICLE

pubs.acs.org/Macromolecules

Cobalt Ferrite Nanoparticles as Multifunctional Cross-Linkers in PAAm Ferrohydrogels

Renate Messing,[†] Natalia Frickel,[†] Lhoussaine Belkoura,[‡] Reinhard Strey,[‡] Helene Rahn,[§] Stefan Odenbach,[§] and Annette M. Schmidt*[,‡]

[†]Institut für Organische Chemie und Makromolekulare Chemie, Heinrich-Heine-Universität Düsseldorf, Universitätsstrasse 1, D-40225 Düsseldorf, Germany

[‡]Department für Chemie, Universität zu Köln, Luxemburger Strasse 116, D-50939 Köln, Germany

[§]Institut für Strömungsmechanik, Professur für Magnetofluiddynamik, Technische Universität Dresden, George-Bähr-Strasse 3, D-01069 Dresden, Germany

ABSTRACT: Ferrohydrogels are synthesized by incorporation of magnetic $CoFe_2O_4$ nanoparticles into a polyacylamide hydrogel network during the polymerization process by utilizing different cross-linking units. Conventional cross-linked ferrohydrogels, using a molecular cross-linker, are compared to those obtained by our new approach where the magnetic particles, surface-functionalized with methacylic groups, serve as sole, multifunctional cross-linkers. Both experimental series are analyzed with regard to their swelling behavior. The novel composite network is examined with respect to the cross-linkage, the network homogeneity, and the network architecture by various experimental techniques.

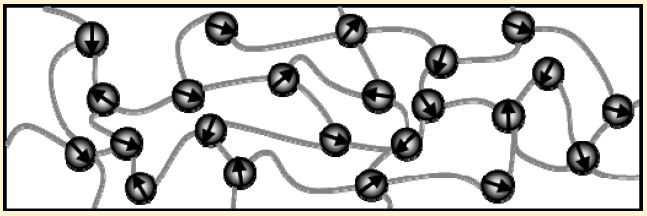

1. INTRODUCTION

The combination of organic and inorganic compounds in nanocomposite materials leads to novel types of materials with a wide range of properties. The integration of inorganic building blocks into three-dimensional hydrogel networks opens the possibility to integrate additional functionalities in these soft and elastic materials.[1−4] In recent years magnetoresponsive hydrogels, so-called ferrohydrogels, received much attention due to the possibility to trigger the properties of the hydrogels remotely controlled by external magnetic fields. Here magnetic nanoparticles incorporated in polymer gel matrices are sensitive to magnetic fields and transfer the involved forces experienced to the surrounding polymer network. This way the dimensions orientation and shape of the hybrid gel can be manipulated by external fields—an effect useful for manufacture soft actuators[5,6] and separation devices.[7,8]

An approach often utilized in the synthesis of ferrohydrogels is cross-linking the gel in the presence of magnetic nanoparticles. The impact of the embedding of iron oxide nanoparticles (Fe_2O_3) to the formation and structure of poly(acrylamide) (PAAm) hydrogels has been investigated in several works.[9,10] In addition, the integration of magnetic nanoparticles (Fe_3O_4) into thermoresponsive hydrogel matrices like poly(*N*-isopropylacrylamide) (PNiPAAm) opens the route for inducing the phase transition of the hydrogel network by heating of the magnetic nanoparticles in an alternating magnetic field.[11] In the mentioned ferrohydrogels, the particle−polymer interaction is mainly related to physicochemical forces.

A chemical, covalent attempt to apply a direct coupling between polymers chains and magnetic nanoparticles is realized by different grafting from polymerization processes, leading to nanoscaled hybrid nanoobjects.[12−14] The magnetic nanoparticles, mostly based on Fe_3O_4, for this purpose are surface functionalized with a siloxane-based shell bearing functional polymerizable groups. By utilizing thermoresponsive polymers like PNiPAAm and poly(oligo(ethylene glycol) methyl ether methacrylate-*co*-methoxyethyl methacrylate) (P(OEGMA-*co*-MEMA)), the dispersion stability of this nanogels can be controlled due to heating the system either by conventional external heating[12,14] or by magnetic heating using an alternating magnetic field.[13] The control of their dispersion stability eases the collection of the nanogels, e.g., through a magnet, and makes them interesting as separation devices.[8]

In macroscopic ferrohydrogels the direct coupling between the polymer matrix and magnetic particles has a number of advantages. The magnetic nanoparticles are entrapped in the polymer network and do not diffuse through or leave the polymer network. In a recently published work, carbonyl-coated magnetic cobalt nanoparticles were surface-functionalized with a vinyl group and integrated covalently in a poly(2-hydroxyethyl methacrylate) (PHEMA) hydrogel network cross-linked by ethylene glycol dimethacrylate (EGDMA) by a free-radical polymerization process.[15] The cobalt particles serve as additional cross-linkers and enhance the stability of the polymer network. In another interesting work, $CoFe_2O_4$ nanoparticles were embedded covalently in a PAAm-based hydrogel.[16] Here, the

Received: November 28, 2010
Revised: March 2, 2011
Published: March 28, 2011

particles were surface-functionalized by a carboxyl group bearing polymerizable poly(ethylene glycol) (PEG). The integration of the particles is achieved by a free-radical polymerization process, and the stability of the network was ensured by the addition of a bifunctional molecular cross-linking reagent. The obtained ferrohydrogels could upload oil-in-water microemulsions into the porous structure of the composite network and this way act as active container for water-based formulations.

In this work, we present the first approach to utilize magnetic nanoparticles as sole, multifunctional cross-linkers in a PAAm-based hydrogel network without an additional use of a conventional molecular cross-linker. The used magnetically blocked $CoFe_2O_4$ nanoparticles are surface-functionalized with a siloxane-based shell bearing unsaturated methacrylic groups, ensuring the covalent coupling with the hydrogel matrix during the polymerization process. We analyze the influence of the $CoFe_2O_4$ particle content on the swelling properties of the particle-linked ferrohydrogels and compare them to the swelling properties of conventional cross-linked ferrohydrogels where the $CoFe_2O_4$ particles are embedded noncovalently. Information on the composition and formation of ferrohydrogels at the different states of swelling was investigated by vibrating sample magnetometry (VSM). Furthermore, the obtained composition of the particle-linked ferrohydrogels, enabling the calculation of the swelling behavior, allows the drawing of conclusions on the architecture of the particle-linked ferrohydrogels.

2. EXPERIMENTAL SECTION

2.1. Chemicals. $FeCl_3 \cdot 6H_2O$, $CoCl_2 \cdot 6H_2O$, $Fe(NO_3)_3$, *N,N′*-methylenebis(acrylamide) (MBA), acrylamide (AAm), and NH_4OH (p.a., 25%), were purchased from Fluka. NaOH (aq, 1 M), HNO_3 (p.a., 63%), and citric acid monohydrate (99.5%) are obtained from Grüssing GmbH. HCl (aq, 1 M) (p.a., Riedel-de-Haën) and tetramethylammonium hydroxide (aq) (Aldrich, 25%) were used as received. Ammonium peroxodisulfate (APDS), *N,N,N′,N′*-tetramethylethylenediamine (TEMED), HF (aq) (p.a. 48%), and $CaCl_2 \cdot 2H_2O$ are obtained from Merck. Methacryloxypropyltrimethoxysilane (MTS, 98%) was purchased from ABCR GmbH. Ethanol and acetone were obtained in technical grade and used after distillation.

2.2. Instrumentation. TEM images of the $CoFe_2O_4$ nanoparticles were taken using a Philipps EM 208S. The samples were prepared by drop-casting on a carbon grid. TEM images of the $CoFe_2O_4$@MTS-linked ferrohydrogels have been carried out with a Zeiss LEO 912 Omega. The sample preparation is done by freeze−fracture direct imaging.[17] The ferrohydrogel was swollen to equilibrium, and a small part of the sample was placed between two grids. After rapid freezing of the sandwich in liquid ethane and fracturing it under liquid nitrogen, one of the grids carrying traces of frozen spicemen was removed from the sandwich and mounted on a cryo-specimen holder precooled at −175 °C and inserted in the microscope. The specimen inside the microscope is surrounded by an anticontaminator metal block permanently cooled with nitrogen reaching a temperature of −175 °C. Freeze-drying of the frozen specimen inside the microscope was effected by allowing the cryo-specimen holder to warm up gradually overnight. X-ray diffraction (XRD) was performed on a Huber Guinier (System 600) diffractometer. Thereby a monochromatic Cu Kα radiation with a wavelength of λ = 1.5406 Å was used. Quasi-static magnetometry was implemented on an ADE Magnetics vibrating sample magnetometer (VSM) EV7. Elemental analysis (EA) of washed and carefully dried particles was carried out with a Perkin-Elmer Analyzer 2400 with an accuracy of measurement of ±0.3%, capable to analyze the elements hydrogen (H), nitrogen (N), and carbon (C). The functionalization density was calculated on behalf of the C content. Dynamic light scattering (DLS) experiments were performed with a Zeta Sizer Nano ZS90 (Malvern Instruments) in water at 25 °C, using 1 × 1 cm^2 polystyrene cuvettes. IR measurements were performed using a FT-IR spectrometer Nicolet 6700 FT-IR equipped with an ATR unit. X-ray tomography was carried out on an instrument developed at the institute of Fluid Mechanics, Chair of Magnetofluiddynamics at TU Dresden. The "LeTo" (low-energy tomography) equipment is based on a commercial cone beam tube emitting a polychromatic X-ray beam with a spot size of 40 μm, a maximal acceleration voltage of 50 kV, and a maximal emission current of 1 mA, allowing the analysis of objects up to 90 mm in width. Further information on the properties and possibilities of this instrument are given elsewhere.[18] For a better visualization the obtained gray values of the 3-dimensional representation of the NP-FHG have been labeled with a color. The measurement of the sample occurred while the swollen ferrohydrogel was involuted into parafilm to avoid drying of the sample by contact with air during the procedure.

2.3. Synthesis of $CoFe_2O_4$ Nanoparticles. The preparation of cobalt ferrite nanoparticles was performed under a nitrogen atmosphere by alkaline precipitation of cobalt chloride and ferric chloride (molar ratio 1:2), based on the method of Massart and Cabuil.[19] The particles were subsequently electrostatically stabilized in aqueous solution by the addition of citric acid (aq, 0.01 M) until the particles flocculate, and redispersion by the addition of tetramethylammonium hydroxide (aq, 25%), leading to a stable ferrofluid of citrate-coated cobalt ferrite nanoparticles that are further addressed in the text as $CoFe_2O_4$@CA.[20]

2.4. Surface Modification of $CoFe_2O_4$ Nanoparticles[12]. A portion of the electrostatically stabilized, water-based $CoFe_2O_4$@CA was added to dry ethanol at a concentration of 2.0 mg mL^{-1}, followed by the addition of ammonium hydroxide 25% solution (0.07 mol per 1 L of ethanol). Afterward, a moderate excess (3.6 mmol per 1 g of cobalt ferrite) of the 3-methacryloxypropyltrimethoxysilane (MTS) solution was added dropwise over a period of 10 min, and the reaction mixture was stirred at ambient temperature for 15 h. Condensation of the siloxane groups on the particle surface was promoted by water removal by azeotropic distillation under reduced pressure. The particles were washed repeatedly with wet acetone by magnetic separation to remove any excess of reagent, citric acid, and salts. Afterward, the $CoFe_2O_4$@MTS nanoparticles were directly redispersed in ethanol. An adequate amount of water was added, and the ethanol was evaporated to obtain a water-based dispersion of MTS-functionalized $CoFe_2O_4$ nanoparticles.

2.5. Synthesis of $CoFe_2O_4$@MTS-Linked PAAm Ferrohydrogels. The $CoFe_2O_4$@MTS-linked ferrohydrogels were synthesized from aqueous particle dispersions and acrylamide (AAm) in a total volume of 2 mL. The composition of the polymerization mixtures is given in Table 1. The monomer (AAm) content of 14 mass % was constant in all samples, and the $CoFe_2O_4$@MTS content was varied. Prior to adding the 2 mg (0.010 mmol) of APDS and 10 μL (0.068 mmol) of TEMED, the dispersions were stored for 15 min at 4 °C. The dispersions were transferred to a teflone form with the measure 2.5 cm × 1.0 cm × 0.2 cm (long × wide × high). The polymerization was initiated by warming up to room temperature, and the reaction was completed within 2 h. The obtained $CoFe_2O_4$@MTS-linked ferrohydrogels were freeze-dried, their weights were determined gravimetrically, and the ferrohydrogels were analyzed via VSM to obtain the composition of the solid material after synthesis. The swelling degree was investigated by immersing the $CoFe_2O_4$@MTS-linked ferrohydrogels in an excess of deionized water until equilibrated and removal of soluble fractions by repeated solvent exchange. The weight of the swollen $CoFe_2O_4$@MTS-linked ferrohydrogels was determined gravimetrically, and the gels were analyzed by VSM, TEM, and X-ray tomography. After the swelling/washing process, the ferrohydrogels were freeze-dried again in order to further analyze the composition and to determine the weight of the nonsoluble fraction gravimetrically.

Table 1. Synthesis Parameter of $CoFe_2O_4$@MTS-Linked Ferrohydrogels and $CoFe_2O_4$@CA Containing MBA-Linked Ferrohydrogels[a]

sample[b]	$\mu_{CoFe_2O_4@CA}$ (mass %)[c]	$\mu_{CoFe_2O_4@MTS}$ (mass %)[c]	μ_{MBA} (mass %)[c]	$\mu_{CoFe_2O_4}/\mu_{AAm}$ (%)[c]
NP-FHG_6.4		0.75		5.08
NP-FHG_7.0		1.00		6.67
NP-FHG_8.2		1.25		8.19
NP-FHG_9.2		1.50		9.68
NP-FHG_9.5		1.75		11.11
NP-FHG_10.8		2.00		12.50
MBA-FHG_0.0	0.00		0.08	0.00
MBA-FHG_5.4	1.25		0.08	8.20
MBA-FHG_6.4	1.50		0.08	9.68
MBA-FHG_7.9	1.75		0.08	11.11
MBA-FHG_10.0	2.00		0.08	12.50

[a] The AAm concentration is kept constant at 14 mass %. [b] NP-FHG: PAAm-based ferrohydrogels cross-linked via $CoFe_2O_4$@MTS nanoparticles. MBA-FHG: MBA-linked ferrohydrogels based on PAAm and $CoFe_2O_4$@CA nanoparticles. Numbers indicate the $CoFe_2O_4$ mass fraction in the dry material after swelling/washing from VSM in mass %. [c] During synthesis.

Scheme 1. Schematic Illustration of the Preparation of $CoFe_2O_4$@CA Containing MBA-Linked Ferrohydrogels (a) and $CoFe_2O_4$@MTS-Linked Ferrohydrogels (b)

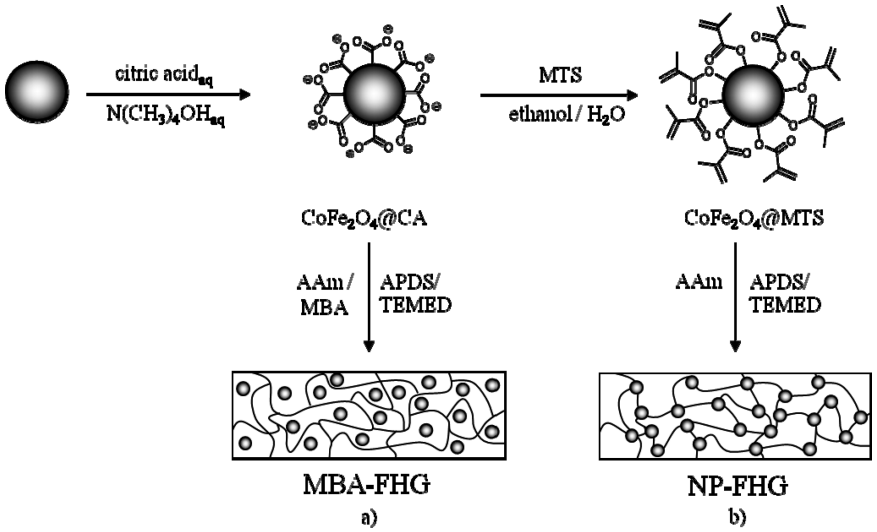

2.6. Synthesis of MBA-Linked $CoFe_2O_4$@CA Containing PAAm Ferrohydrogels. The synthesis of MBA-linked ferrohydrogels occurred in full analogy to section 2.5, with the exception that citrate-stabilized $CoFe_2O_4$@CA particles were used, and MBA was added as a cross-linker. The composition of the polymerization mixture is shown in Table 1. The monomer (AAm) content of 14 mass % and the cross-linker content (MBA) of 0.08 mass % were constant in all samples, and the $CoFe_2O_4$@CA content was varied. Workup and analysis are in full accordance with the procedure described above (section 2.5).

3. RESULTS AND DISCUSSION

The integration of magnetic nanoparticles into hydrogel matrices allows the combination of magnetic properties with the mechanical properties of the polymer network. In the present work we investigate the possibility to incorporate the nanoparticles homogeneously into a polyacrylamide (PAAm) network by two different methods. The conventional and well-known pathway to embed nanoparticles in such a network is to integrate them into a conventional molecular cross-linked hydrogel during the polymerization process.[9] In our novel approach we aim at integrating the nanoparticles by a direct coupling to the polymer chains and to use them as multifunctional cross-linkers. By comparing the swelling behavior of the two experimental series, we obtain information on the network architecture and formation. The utilization of magnetically blocked $CoFe_2O_4$ nanoparticles, which reorientate in outer magnetic fields by Brownian mechanical rotation, opens the possibility to influence the composite network by applying outer magnetic fields in further applications.

3.1. Properties of $CoFe_2O_4$ Nanoparticles. The $CoFe_2O_4$ we utilized to synthesize the ferrohydrogels have several advantages. On the one hand, the synthesis procedure leads to particles with reproducible properties in size and form. The synthesis can be scaled up so that the particles are available in high amounts. In addition, their dispersion behavior in water and in other polar solvents makes them interesting for further applications. On the other hand, due to their blocked magnetic behavior, they show

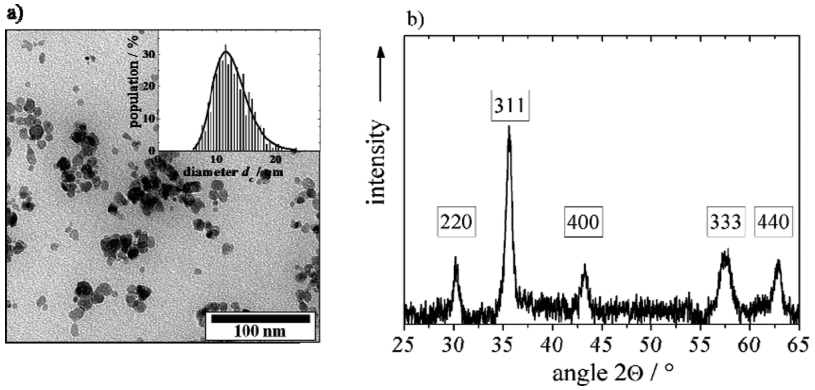

Figure 1. (a) TEM image of $CoFe_2O_4$ nanoparticles with core size distribution histogram (inset). (b) X-ray diffractogram of bare $CoFe_2O_4$ nanoparticles and assigned *hkl* indices.

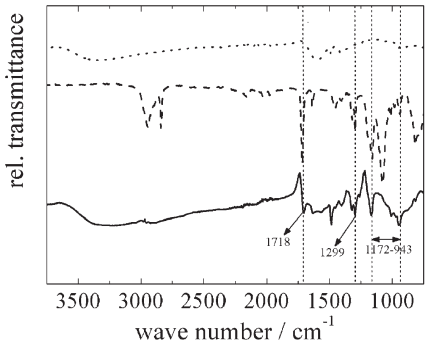

Figure 2. ATR-FTIR spectra of $CoFe_2O_4$ nanoparticles before surface functionalization (dotted line), $CoFe_2O_4$@MTS nanoparticles (solid line), and the MTS reagent (dashed line).

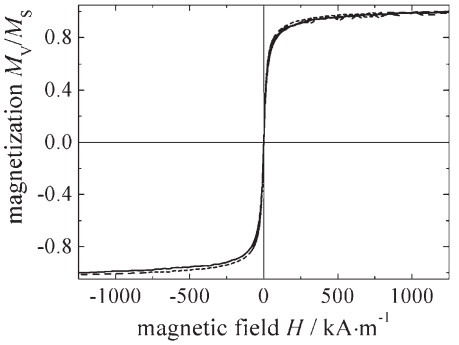

Figure 3. Quasi-static magnetic properties of $CoFe_2O_4$@CA aqueous ferrofluid (μ = 2.61 mass %; solid line) and $CoFe_2O_4$@MTS aqueous ferrofluid (μ = 2.08 mass %; dashed line).

magneto-mechanical coupling that allows insight into the local interactions between particles and matrix as will be addressed in an upcoming paper. The particles were obtained by alkaline precipitation following Massart's method[19] and stabilized electrostatically with citric acid and tetramethylammonium hydroxide in water,[20] leading to a stable aqueous ferrofluid of $CoFe_2O_4$ nanoparticles.

From the TEM image (Figure 1a), a mean core diameter of d_c = 12.2 nm (σ = 0.23) was extraced from log-normal distribution fitting of the histogram. In X-ray diffraction (XRD) experiments (Figure 1b) the inverse spinel structure of $CoFe_2O_4$ is confirmed, and the peaks could be assigned to the *hkl* indices. Because of the small crystal size, the lines show considerable broadening, and by using the Scherrer equation,[21] we calculate a volume-average crystallite diameter of 12.4 nm. The good accordance with the mean particle diameter obtained in TEM confirms the high crystallinity and the monodomain character of the individual particles.

For further utilization in the particle-linked ferrohydrogels, the citrate-stabilized particles are surface-functionalized with methacryloxypropyltrimethoxysilane (MTS). By addition of the functionalization reagent to an ethanol-based dispersion of the $CoFe_2O_4$@CA particles, the MTS forms a thin siloxane-based layer on the particles surface through condensation of the alkoxy groups.[12] The surface modification can be monitored qualitatively by ATR-FTIR spectroscopy, while quantitative information can be obtained by EA. In Figure 2, IR spectra of $CoFe_2O_4$ nanoparticles before surface functionalization, of $CoFe_2O_4$@MTS nanoparticles, and of the MTS reagent are shown. The spectra of $CoFe_2O_4$@MTS nanoparticles and MTS indicate a significant vibrational absorption of the Si−CH_2 bond in the fingerprint region 1326 and 1299 cm^{-1}, in agreement with the literature.[22,23] Another characteristic signal can be attributed to the asymmetric −Si−O−Si− vibration between 1172 and 943 cm^{-1}.[24,25] In addition, the spectrum of the methacryloxy group-bearing particles shows the vibrational absorption of the carbonyl double bond at 1718 cm^{-1}. The vibrational absorption of the C−H bonding of methoxy groups of pure MTS at 2943 and 2841 cm^{-1} are not found in the spectrum of $CoFe_2O_4$@MTS, in accordance with the hydrolysis of the methoxysilane groups and condensation to the particle surface.

From the carbon content in the dried particle powder obtained from EA, we calculate a specific particle functionality of 1.1 mmol g^{-1}. Taking into account the particles size d_c = 12.2 nm from TEM and a density of $CoFe_2O_4$ of ρ = 5.3 g cm^{-3},[26] we estimate a surface coverage of 7.1 molecules MTS per nm^2 of the particle surface, leading to around 3300 methacrylic groups per particle. The high amount of functional groups on the particles surface implied that the $CoFe_2O_4$@MTS particles are able to serve as multifunctional cross-linkers in the particle-linked ferrohydrogels.

To obtain homogeneous ferrohydrogels with a unique distribution of the $CoFe_2O_4$ particles inside the polymer network, it is necessary that the particles are good dispersible in water. The dispersion stability of the $CoFe_2O_4$@CA and $CoFe_2O_4$@MTS particles in water is investigated by DLS measurements.

Table 2. Composition, Gel Content, and Swelling Degree of $CoFe_2O_4$@MTS-Linked Ferrohydrogels (NP-FHG) and MBA-Linked Ferrohydrogels (MBA-FHG)

	dried ferrohydrogel after work-up	ferrohydrogel at equilibrium swelling		gel content	swelling degree
sample[a]	$\mu_{CoFe_2O_4,d}$ (mass %)[b]	$\mu_{CoFe_2O_4,q}$ (mass %)[b]	$\mu_{PAAm,q}$ (mass %)[c]	G (%)[d]	$Q_{v,PAAm}$[e]
NP-FHG_6.4	6.44	0.10	1.44	94.1	90.0
NP-FHG_7.0	7.00	0.22	2.92	>99	44.1
NP-FHG_8.2	8.16	0.32	3.19	95.8	40.3
NP-FHG_9.2	9.18	0.48	5.04	>99	25.4
NP-FHG_9.5	9.51	0.51	4.89	97.5	26.1
NP-FHG_10.8	10.83	0.74	6.08	>99	20.9
MBA-FHG_0.0	0.00	0.00	4.47	90.0	28.8
MBA-FHG_5.4	5.44	0.26	4.53	>99	28.3
MBA-FHG_6.4	6.49	0.30	4.31	>99	29.8
MBA-FHG_7.9	7.89	0.39	4.51	>99	28.4
MBA-FHG_10.0	9.99	0.54	4.37	>99	29.3

[a] For sample annotations see Table 1 footnote. [b] From VSM. [c] After $\mu_{PAAm,q}/\mu_{CoFe_2O_4,q} = \mu_{PAAm,d}/\mu_{CoFe_2O_4,d}$. [d] From gravimetry. [e] After eq 2.

Both $CoFe_2O_4$@CA and $CoFe_2O_4$@MTS indicate a hydrodynamic diameter of 13.7 nm, proving that the particle size is not significantly altered in the course of the functionalization process, in agreement with the absence of particle agglomeration, multilayer formation, and secondary particle nucleation. Together with EA results, the data indicate the formation of a reaction-site- and monomer-size-limited monolayer of MTS on the particle surface.

The findings are confirmed in quasi-static magnetization experiments, where both samples showed pseudo-superparamagnetic behavior in the dispersed state indicated by absence of hysteresis (coercivity values <0.25 kA m^{-1}; see Figure 3).[27]

On the basis of theoretical and experimental results,[28] the critical diameter for the superparamagnetic/ferromagnetic transition for $CoFe_2O_4$ nanoparticles amounts to around 5 nm at room temperature. In other words, the free rotation of magnetic moments of the particles within the crystal lattice is hindered. Therefore, it can be assumed that a high volume fraction of particles are single-domain dipolar particles with a considerable ferromagnetic blocking. Monodispersed in a fluid of low viscosity, such particles rotate by Brownian motion. As a result of this, the coercive field strength diminishes, and the particle ensemble shows pseudo-superparamagnetic behavior in quasi-static magnetization experiments.

By applying Chantrells method[29] based on the Langevin equation, we extract information on the $CoFe_2O_4$ content and the volume average core size of the particles. The results for $CoFe_2O_4$@CA and $CoFe_2O_4$@MTS water-based dispersions indicate a content $\mu_{CoFe_2O_4}$ of 2.61 and 2.08 mass %, with a volume average diameter d_v of 12.4 and 12.2 nm, respectively. The good coincidence with the average core diameter obtained by TEM and XRD indicates that the cores react individually to the applied field and thus that they are individually dispersed and do not show agglomeration upon field application.

3.2. Determination of the Ferrohydrogel Composition. To understand the impact of particles on the network formation and to verify their architecture, we compared two series of ferrohydrogels based on different cross-linking species. In the one case, we used $CoFe_2O_4$@MTS nanoparticles to serve as multifunctional cross-linkers in the composite material by applying a covalent coupling between the particles and the polymer chains. In the other case, the $CoFe_2O_4$@CA nanoparticles were embedded noncovalently in a conventionally chemically cross-linked polymer network by applying a molecular tetrafunctional cross-linking reagent (MBA). In both series of experiments, the monomer content was kept constant, and the particle content was varied. In the case of MBA-linked ferrohydrogels, the cross-linker concentration was also kept constant. The chosen composition conditions enable us to analyze the impact of the $CoFe_2O_4$ content on the swelling behavior in the two series with different kinds of cross-linking.

After the synthesis the samples of both experimental series were freeze-dried, followed by swelling/extraction cycles in an excess of deionized water in order to remove soluble material and to determine the equilibrium swelling degree. While the gel content was determined gravimetrically, the swelling degree was obtained from VSM composition results (see below).

In the case of the MBA cross-linked ferrohydrogels, we obtain form-stable and well-cross-linked ferrohydrogels. The swelling reagent changed its color to slightly brown in all samples, indicating that only a small fraction of particles can escape the polymer network. Similarly, we observed an equilibrium swelling behavior of well-defined, permanent gels in the case of the particle-linked ferrohydrogels, although no additional, conventional molecular cross-linking reagent was involved. The high stability of the gels when immersed in water, or water/alcohol, water/acetone, and water/DMF mixtures, indicates a permanent (chemical) cross-linking. In contrast, most physical gels that gelate due to microphase separation or H-bonds disassemble in nonselective solvent mixtures or upon the addition of DMF as H-bond concurrent. In a blind test under the same synthesis conditions but without $CoFe_2O_4$@MTS particles, the polymer network disappears during the swelling process.

From the determined weight of the solid content of the ferrohydrogels after synthesis $m_{s,d}$ and after swelling m_d we could analyze the gel content G, which is a measure for the fraction of reagents permanently bond to the composite network (eq 1). All gel contents are higher than 90%, and in most cases, no weight loss is detected at all. As in all NP-FHG, the swelling/washing fractions stayed colorless with no detectable magnetic residues; we conclude that all particles are bound in the composite network, and weight loss in the swelling/washing process thus

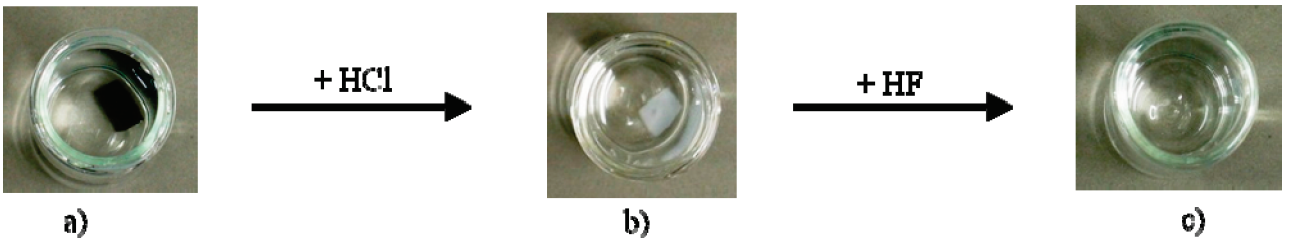

Figure 4. Photographs of the swollen NP-FHG_10.8 before the dissolution experiments (a), the hydrogels after addition of hydrochloric acid and washing (b), and the polymer solution after addition of hydrofluoric acid (c).

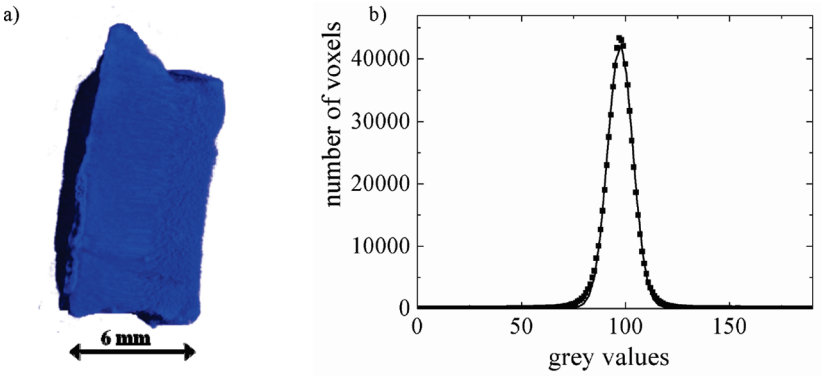

Figure 5. X-ray tomogram of the swollen NP-FHG_10.8 (a) and the accordant histogram, obtained by plotting the number of voxels calculated within the digital data set against the gray values (b).

is due to loss of polymer that is not included into the macroscopic networks. This fraction is low, though, and decreases with increasing particle content.

From VSM results of the dried samples after work-up, we obtain the particle-to-polymer ratio, and this allows to calculate the composition of ferrohydrogels in the swollen state.

$$G = \frac{m_{s,d}}{m_d} \quad (1)$$

In Table 2, the respective gel compositions of NP-FHG and MBA-FHG in the swollen state and in the dried state are summarized together with gel content G and the swelling degree $Q_{v,PAAm}$. The swelling degrees are discussed in section 3.5.

3.3. Employment of Nanoparticles as Multifunctional Cross-Linkers. In order to confirm that the cross-linking in the NP-FHG series is based on the MTS-modified nanoparticles serving as multifunctional cross-linkers, we carried out a dissolution experiment in two steps aiming at the selective disintegration of the inorganic cross-linking units using mineral acids. At first, 0.5 mL of aqueous hydrochloric acid is added to a probe of water-swollen, black NP-FHG_10.8 (Figure 4a). The color of the ferrohydrogel and of the swelling reagent turned immediately to light green due to the dissolution of the $CoFe_2O_4$ and the release of the iron and cobalt ions. Repeated washing cycles with deionized water results in a turbid and colorless hydrogel of the same size of the initial ferrohydrogel (Figure 4b). The dimensions of the hydrogel are retained in this first step due to the present of the siloxane-based shell of the $CoFe_2O_4$@MTS nanoparticles that resists the hydrochloric acid treatment. In a second step, a few drops of aqueous hydrofluoric acid are added to the hydrogel matrix. After less than 1 h the turbit hydrogel is dissolved, and a clear and colorless solution is obtained (Figure 4c). Hydrofluoric acid is known to attack Si−O−Si bonds, and as a result, the hydrogel fully disintegrates.

In a comparable dissolution experiment with MBA-FHG, we could observe a stable hydrogel matrix after the dissolution of the particles with hydrochloric acid, and treatment with hydrofluoric acid, indicating that the MBA-mediated cross-links in these networks are not attacked.

3.4. Network Morphology and Architecture of Particle-Linked Ferrohydrogels. To investigate the network morphology and architecture of the NP-FHG, we analyzed them in the swollen state in TEM, while the homogeneity of the composite network had been explored in X-ray microcomputed tomography.

In the X-ray tomography it is possible to investigate the homogeneity of the composite network with a micrometer range resolution. After the measurement the 2-dimensional projections have been reconstructed to a 3-dimensional representation of the ferrohydrogel using a cone beam reconstruction algorithm established by Feldkamp.[30] Subsequently, an analysis of the digital data set has been carried out using the VGStudio Max and ImageJ software. In Figure 5a, the X-ray tomogram of a swollen NP-FHG network is shown. In the 3-dimensional representation the uniform blue color confirms the high homogeneity of the NP-FHG. In Figure 5b the corresponding histogram of the rendered representation of the ferrohydrogel is shown with a narrow gray value distribution. Using a Gaussian fit, the mean gray value is determined as 97.45 with a standard deviation σ_G = 6.04. The low deviation confirms the high homogeneity of the swollen NP-FHG network.

The TEM images of NP-FHG shown in Figure 6 are obtained by freeze−fracture direct imaging.[17] Therefore, the swollen

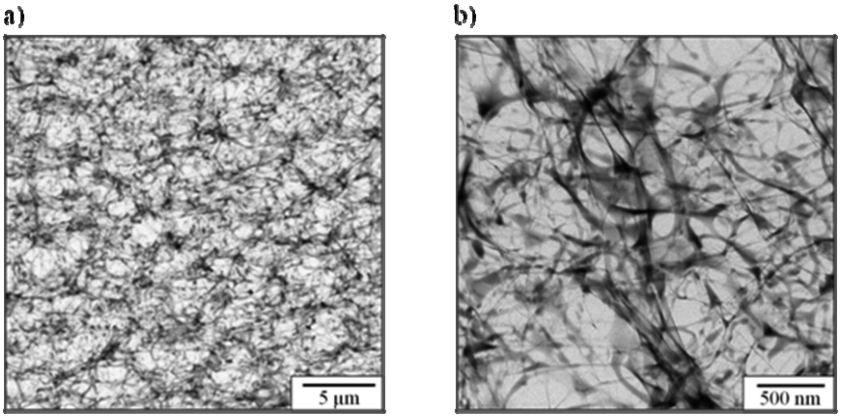

Figure 6. TEM images of a swollen, freeze-fractured, freeze-dried NP-FHG_10.8 at different resolutions.

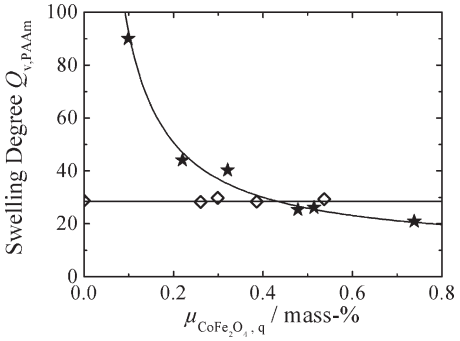

Figure 7. Volume-based swelling degree $Q_{v,PAAm}$ of NP-FHG (stars) and MBA-FHG (rhombus) plotted against the $CoFe_2O_4$ content in the swollen state.

samples are frozen between two grids and fractured by dividing the sandwich-formed sample. The NP-FHG were freeze-dried at $T = -175$ °C in high vacuum in order to prevent a shrinkage of the network. In Figure 6, the microscopic homogeneous composition of the network is clearly visible, and the structural features of the network, regarding the mesh size and the nature of the junction points, become observable. Although an exact analysis of the mesh size and the node distance is not possible due to the two-dimensional projection of a three-dimensional object, we estimate a mesh size range of 150 nm. The dark points found at the nodes confirm that the particles are localized at the segment cross-links.

3.5. Swelling Behavior of Ferrohydrogels. One of the major properties of hydrogels is their ability to swell by taking up a multiple volume of water. Thereby, the equilibrium swelling degree depends on the interaction parameter of the polymer and water and the cross-linking density. The higher the cross-linking density of a given network system, the lower is the swelling ability due to entropic limitations. In the reported hybrid particle-linked ferrohydrogels, the impact of the $CoFe_2O_4$@MTS particle cross-linkers on the equilibrium swelling degree is analyzed. Similarly, we analyzed the impact of citrate-stabilized particles on the swelling behavior of conventionally, MBA-linked ferrohydrogels. Therefore, both series of ferrohydrogels were immersed in an excess of deionized water. Volume-based swelling degrees $Q_{v,PAAm}$ of the polymer fraction were calculated from VSM results of the swollen and dried ferrohydrogels using eq 2 by taking into account that the particle core volume stays constant during swelling, i.e., only the polymer fraction swells. We use mass-based compositions, as the volume of freeze-dried samples is not easily determined due to its porous structure (see also Figure 6) and transfer it to the volume-based swelling degree using density values for water and PAAM from the literature. The swelling degree of the pure MBA-linked hydrogel (MBA-FHG 1) without nanoparticles is analyzed gravimetrically using eq 5. In Figure 7, the volume-based swelling degrees $Q_{v,PAAm}$ for the two series of ferrohydrogel are plotted against the $CoFe_2O_4$ content in the swollen state.

$$Q_{v,\,PAAm} = 1 + \rho_2\left(\frac{\mu_{H_2O,\,q} + \mu_{PAAm,\,q}}{\mu_{PAAm,\,q}\rho_1} - \frac{1}{\rho_1}\right) \quad (2)$$

where ρ_1 is the density of the swelling medium (1.0 g cm^{-3}), ρ_2 the density of PAAm (1.35 g cm^{-3}), $\mu_{PAAm,q}$ the mass fraction of PAAm in the swollen ferrohydrogel (in mass %), and $\mu_{H_2O,q}$ the mass fraction of water in the swollen ferrohydrogel (in mass %)). The mass fractions are calculated as follows.

$$\mu_{PAAm,\,q} = \frac{\mu_{CoFe_2O_4,\,q}}{\mu_{CoFe_2O_4,\,d}}\mu_{PAAm,\,d} \quad (3)$$

$$\mu_{H_2O,\,q} = 100 - \mu_{PAAm,\,q} - \mu_{CoFe_2O_4,\,q} \quad (4)$$

$$Q_{v,\,PAAm} = 1 + \rho_2\left(\frac{m_q}{m_d\rho_1} - \frac{1}{\rho_1}\right) \quad (5)$$

where m_q is the mass of the swollen ferrohydrogel and m_d the mass of the dried polymer network after swelling.

The swelling degree $Q_{v,PAAm}$ in the NP-FHG increases with decreasing $CoFe_2O_4$ content while the swelling ability in the MBA-linked ferrohydrogels is nearly independent of the $CoFe_2O_4$ content. In the latter case, this indicates that the particles' presence does not have a significant influence on the network formation and structure despite the hydrophilic (charged) nature of the particle surface. Here it has to be taken into account that the volume fraction of particles is below 2 vol % with respect to the polymer phase, so that the contribution to the overall swelling is low.

In contrast, in particle-linked networks, the observed impact of the particle content on the swelling behavior in NP-FHG is an additional evidence for the particles' impact on the cross-linking

density. The correlation of the equilibrium swelling degree $Q_{v,PAAm}$ and the cross-linker can be approximated with a hyperbolic decay (eq 6), taking into account the limit of the swelling conditions employed during synthesis, $Q_{v,PAAm,s}$, of 9.3.

$$Q_{v,\,PAAm} = \frac{C}{\mu_{CoFe_2O_4,\,q}} + Q_{v,\,PAAm,\,s} \tag{6}$$

The constant C depends under more on the specific cross-linker functionality f of the particles. For the multifunctional particles this value is not directly accessible, so it will be further addressed in more detail together with the corresponding segment length M_c.

For the calculation, we utilized two different approaches. Both approaches are based on eq 7, correlating the monomer mass per particle m_{AAm}/n_{NP} to the product of the segment length M_c and the number of chains per particle by means of the average cross-linker functionality f.

$$\frac{m_{AAm}}{n_{NP}} = M_c \frac{f}{2} \tag{7}$$

In the first approach $Q_{v,PAAm}$ is used to calculate f and M_c by utilizing the generalized Flory–Rehner model in an iteration procedure (eq 8).[31,32] The model was found to fit well to conventional MBA-linked PAAm hydrogels. Therefore, we used the model to estimate the network parameter in the NP-FHG. Equation 7 enables the calculation of M_c by the knowledge of the swelling degree of the polymer network under synthesis conditions and at equilibrium swelling.

$$M_c = \left(1 - \frac{2}{f}\right) V_1 \rho_2 \frac{\frac{2}{f} \nu_{2,q} - {\nu_{2,s}}^{2/3} {\nu_{2,q}}^{1/3}}{\ln(1-\nu_{2,q}) + \nu_{2,q} + \chi {\nu_{2,q}}^2} \tag{8}$$

where M_c is the average segment length (g mol^{-1}), f the cross-linker functionality, V_1 the molar volume of the solvent water (18 cm^3 mol^{-1}), ρ_2 the density of the polymer (1.35 g cm^{-3}), $\nu_{2,q}$ the volume fraction of PAAm in the swollen state ($1/Q_{v,PAAm}$), $\nu_{2,s}$ the volume fraction of PAAm under synthesis conditions, and χ the Flory–Huggins interaction parameter (0.47 for PAAm/water).[33]

The second approach to obtain information on the network parameter f and M_c is due to the calculation of the particle distance r_{NP} in the swollen NP-FHG from the known number-density of particles n_{NP} (eq 9). In Figure 8, the particle distance r_{NP} of the swollen NP-FHG is plotted against the $CoFe_2O_4$ content.

$$r_{NP} = \left(\frac{1}{n_{NP}}\right)^{1/3} \tag{9}$$

The obtained values for the particle distance r_{NP}, shown in Figure 8, are in good agreement with the TEM images in Figure 6 taken from a freeze-dried ferrohydrogel.

From the obtained particle distance r_{NP} the segment chain length M_c can be calculated from the Flory mesh size at Θ conditions (eq 10), taking into account the Flory–Huggins interaction parameter χ for PAAm/water (0.47) is close to the Θ value of 0.5.

$$M_c = M_{AAm} N_c = M_{AAm} \left(\frac{r_{NP}}{2}\right)^2 \tag{10}$$

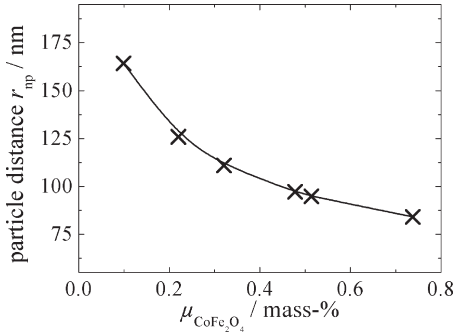

Figure 8. Particle distance r_{NP} of the NP-FHG plotted against the $CoFe_2O_4$ content in the swollen state (the line is a guide to the eye).

Scheme 2. Feasible Model of the Network Architecture for the $CoFe_2O_4$@MTS-Linked Ferrohydrogels

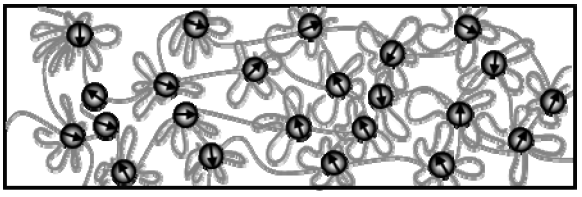

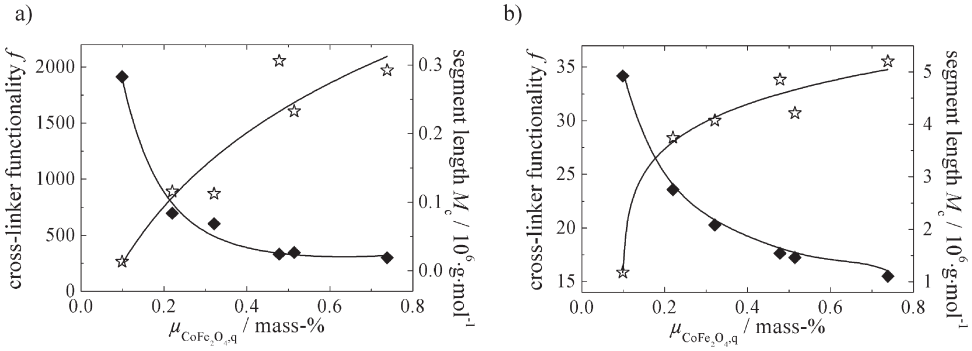

Figure 9. Cross-linker functionality f (stars) and the segment length M_c (rhombus) in NP-FHG calculated by the Flory–Rehner model (a) and the particle distance model (b) plotted against the $CoFe_2O_4$ content in the swollen state (the lines are a guide to the eye).

dx.doi.org/10.1021/ma102708b |*Macromolecules* 2011, 44, 2990–2999

The calculated values for M_c and f obtained by the two different approaches are shown in Figure 9a,b. Both approaches show a comparable increase of the cross-linker functionality f and a decrease of the segment length M_c with increasing $CoFe_2O_4$@MTS content, but the values obtained by the two approaches are of different magnitudes. From the first approach (Flory−Rehner model) we obtain high average cross-linker functionalities f in the order of 260−2000 and relative small average segment length M_c between 20 000 and 300 000 g mol^{-1}. The latter values are much smaller than expected from the particle distance r_{NP}. Accordingly, we obtained a lower cross-linker functionality f in the order of 16−36 and a higher segment length M_c between 1 100 000 and 5 000 000 g mol^{-1}, when we take this into account.

The above-mentioned results, which draw varying pictures of the network structure, lead us to the following feasible architecture as shown in Scheme 2, which unifies the apparently different findings. The particle distance r_{NP} in the NP-FHG points out that the $CoFe_2O_4$@MTS nanoparticles are linked by long PAAm polymer segments which is confirmed by the calculated M_c from this approach. The corresponding low cross-linker functionality f displays that the fraction of these long polymer chains, which are attached to two particles, on the total polymer fraction is small. On the other hand, the high cross-linker functionality f and the lower segment length M_c obtained by the Flory−Rehner model indicate that a fraction of shorter polymer segments is present, attached to the same particle on both ends, thus forming loops around the particles. These polymer fractions contribute to the swelling behavior, but not to a direct linkage between adjacent particles.

4. CONCLUSION

Ferrohydrogels composed of a PAAm matrix containing $CoFe_2O_4$ nanoparticles were synthesized which are incorporated in the hydrogel matrix through different cross-linking approaches. We examined the possibility to utilize methacrylic surface-functionalized $CoFe_2O_4$ nanoparticles as sole, multifunctional cross-linkers in the ferrohydrogels, providing a direct covalent coupling between the magnetic particles and the polymer chains. The other experimental series was composed of embedding the $CoFe_2O_4$ nanoparticles noncovalently into a conventional cross-linked ferrohydrogels using a molecular, tetrafunctional cross-linking reagent. The composition and the swelling degree of the two experimental series were investigated by vibrating sample magnetometry (VSM). The homogeneity of the particle-linked ferrohydrogel network was proven by TEM and X-ray tomography. In dissolution experiments we could prove the cross-linking in the particle-linked ferrohydrogels based on the methacylic-functionalized siloxane-based shell of the particles.

The analysis of the swelling degree of the two experimental series of ferrohydrogels in dependence of the $CoFe_2O_4$ content enables the analysis of influence of the particles on the network formation and architecture. In the conventional cross-linked ferrohydrogels the swelling degree was independent of the particle content, indicating that the embedded particles do not influence the network formation. In the particle-linked ferrohydrogels we found a decrease of the swelling degree with increasing $CoFe_2O_4$ content comparable to the influence of cross-linker concentration on the swelling degree observed in conventional, chemical cross-linked hydrogels. Furthermore, we gained additional information from the swelling degree on the network parameter like the cross-linker functionality of the $CoFe_2O_4$ particles and the segment length of the polymer chains in the particle-linked ferrohydrogels by using different approaches.

This leads us to a model of a feasible network architecture where the particles are linked by a few long chains while a high fraction of smaller polymer chains form loops around single particles and do not contribute to the network strength.

Our novel approach of cross-linking a ferrohydrogels network by the covalent coupling of the magnetic nanoparticles to the polymer chains opens the possibility to analyze the particles direct environment by examining their magnetic behavior. This way a better insight into the processes of particles motion and the particle-to-polymer interaction can be achieved.

■ ACKNOWLEDGMENT

We thank Prof. R. Yerushalmi-Rozen (Ben Gurion-University - Israel) for TEM imaging of the $CoFe_2O_4$ nanoparticles and Prof. Frank (Heinrich-Heine-Universität Düsseldorf) for X-ray diffractometry. We gratefully acknowledge the DFG (SPP1259 and Emmy Noether-Program) for financial support.

■ REFERENCES

(1) Kickelbick, G. Hybrid Materials. Synthesis, Characterization, and Applications, Wiley-VCH: Weinheim, 2007.
(2) Kopecek, J. *J. Polym. Sci., Part A: Polym. Chem.* **2009**, *47*, 5929–5946.
(3) Messing, R.; Schmidt, A. M. *Polym. Chem.* **2011**, *2*, 3–14.
(4) Schexnailder, P.; Schmidt, G. *Colloid Polym. Sci.* **2009**, *287*, 1–11.
(5) Ramanujan, R. V.; Lao, L. L. *Smart Mater. Struct.* **2006**, *15*, 952.
(6) Snyder, R. L.; Nguyen, V. Q.; Ramanujan, R. V. *Smart Mater. Struct.* **2010**, *19*, 055017.
(7) Daniel Horák, M. B.; Hana Macková, M. J. B. *J. Sep. Sci.* **2007**, *30*, 1751–1772.
(8) Gelbrich, T.; Reinartz, M.; Schmidt, A. M. *Biomacromolecules* **2010**, *11*, 635–642.
(9) Galicia, J. A.; Cousin, F.; Dubois, E.; Sandre, O.; Cabuil, V.; Perzynski, R. *Soft Matter* **2009**, *5*, 2614–2624.
(10) Mayer, C. R.; Cabuil, V.; Lalot, T.; Thouvenot, R. *Adv. Mater.* **2000**, *12*, 417.
(11) Ramanujan, R. V.; Ang, K. L.; Venkatraman, S. *J. Mater. Sci.* **2009**, *44*, 1381–1387.
(12) Frickel, N.; Messing, R.; Gelbrich, T.; Schmidt, A. M. *Langmuir* **2009**, *26*, 2839–2846.
(13) Gelbrich, T.; Marten, G. U.; Schmidt, A. M. *Polymer* **2010**, *51*, 2818–2824.
(14) Sun, Y. B.; Ding, X. B.; Zheng, Z. H.; Cheng, X.; Hu, X. H.; Peng, Y. X. *Chem. Commun.* **2006**, 2765–2767.
(15) Fuhrer, R.; Athanassiou, E. K.; Luechinger, N. A.; Stark, W. J. *Small* **2009**, *5*, 383–388.
(16) Bonini, M.; Lenz, S.; Falletta, E.; Ridi, F.; Carretti, E.; Fratini, E.; Wiedenmann, A.; Baglioni, P. *Langmuir* **2008**, *24*, 12644–12650.
(17) Belkoura, L.; Stubenrauch, C.; Strey, R. *Langmuir* **2004**, *20*, 4391–4399.
(18) Brunke, O.; Odenbach, S.; Jurgons, R.; Alexiou, C.; Hilger, I.; Beckmann, F. *J. Phys.: Condens. Matter* **2006**, *18*, 2903–2917.
(19) Massart, R.; Cabuil, V. *J. Chim. Phys. Phys.-Chim. Biol.* **1987**, *84*, 967–973.
(20) van Ewijk, G. A.; Vroege, G. J.; Philipse, A. P. *J. Magn. Magn. Mater.* **1999**, *201*, 31–33.
(21) Scherrer, P. *Nachr. Ges. Wiss. Göttingen, Math.-Phys.* **1918**, *Kl. 2*, 98.
(22) Miller, J. D.; Ishida, H. *J. Chem. Phys.* **1987**, *86*, 1593–1600.
(23) Williams, H. D.; Fleming, I. *Strukturaufklärung in der Organischen Chemie*; Thieme: Stuttgart, 1991.

(24) Hall, S. R.; Davis, S. A.; Mann, S. *Langmuir* **2000**, *16*, 1454–1456.
(25) Miller, J. D.; Ishida, H. *Surf. Sci.* **1984**, *148*, 601–622.
(26) Landolt-Börnstein, Ed.; *Zahlenwerte und Funktionen*; Springer-Verlag: Berlin, 1970.
(27) Rosensweig, R. E. *Ferrohydrodynamics*, 1st ed.; Cambridge University Press: New York, 1985.
(28) Veverka, M.; Veverka, P.; Kaman, O.; Lancok, A.; Zaveta, K.; Pollert, E.; Knizek, K.; Bohacek, J.; Benes, M.; Kaspar, P.; Duguet, E.; Vasseur, S. *Nanotechnology* **2007**.
(29) Chantrell, R.; Popplewell, J.; Charles, S. *IEEE Trans. Magn.* **1978**, *14*, 975–977.
(30) Feldkamp, L. A.; Davis, L. C.; Kress, J. W. *J. Opt. Soc. Am.* **1984**, *1*, 612–619.
(31) Flory, P. J.; Rehner, J. *J. Chem. Phys.* **1943**, *11*, 521–526.
(32) Mark, J. E. *Rubber Chem. Technol.* **1982**, *55*, 762–769.
(33) *Polymer Data Handbook*; Oxford University Press: New York, 1999.